A Tabulated-Chemistry Approach applied to a Quasi-Dimensional Combustion Model for a Fast and Accurate Knock Prediction in Spark-Ignition Engines

Author, co-author (Do NOT enter this information. It will be pulled from participant tab in MyTechZone)

Affiliation (Do NOT enter this information. It will be pulled from participant tab in MyTechZone)

Abstract

The description of knock phenomenon is a critical issue in a combustion model for Spark-Ignition (SI) engines. The most known theory to explain this phenomenon is based on the Auto-Ignition (AI) of the end-gas, ahead the flame front. The accurate description of this process requires the handling of various aspects, such as the impact of the fuel composition, the presence of residual gas or water in the burning mixture, the influence of cool flame heat release, etc. This concern can be faced by the solution of proper chemistry schemes for gasoline blends. Whichever is the modeling environment, either 3D or 0D, the on-line solution of a chemical kinetic scheme drastically affects the computational time.

In this paper, a procedure for an accurate and fast prediction of the hydrocarbons auto-ignition, applied to phenomenological SI engine combustion models, is proposed. It is based on a tabulated approach, operated on both ignition delay times and reaction rates. This technique, widely used in 3D calculations, is extended to 0D models to overcome the inaccuracies typical of the most common ignition delay approaches, based on the Livengood-Wu integral solution.

The aim is to combine the predictability of a detailed chemistry with an acceptable computational effort. First, the tabulated technique is verified through comparisons with a chemical solver for a semi-detailed kinetic scheme in constant-pressure and constant-volume configurations. Then a phenomenological model, based on the end-gas AI computation, is utilized to predict the knock occurrence in different SI engines, including both naturally-aspirated and turbocharged architectures. 0D/1D simulations are performed both with an online solution of the chemistry and employing the tabulated approach. Assessment with reference $KLSA$ values shows that the knock model, based on the tabulated chemistry, is able to well reproduce the essential features of the auto-ignition process in the analyzed engines, with a limited impact on the computational time.

Introduction

"Normal" heat release in Spark-Ignition (SI) Internal Combustion Engines (ICE) is controlled by the flame propagation, initiating at the spark plug electrodes and developing inside the combustion chamber. Mainly depending on the pressure and temperature history of the unburned mixture, "abnormal" combustions, such as knock, can also occur. As known, knock is the harmful consequence of the self-ignition of a portion of unburnt mixture (end-gas), before it is consumed by the main propagating flame front [1]. If left untreated, engine knock determines a series of major drawbacks. First, pressure oscillations, induced by the sudden end-gas heat release, break the film of lubricant placed on the cylinder walls, with consequent increase in the coefficient of heat transfer, thermal energy losses, and engine seizure. Moreover, the strong increase in thermal and mechanical stresses may also lead to valve damages and to the fusion of the piston head [1,2].

To avoid the knock onset, engine geometrical and operating parameters are properly defined at design and calibration engine stages, respectively. To limit the pressure and temperature peaks, the geometrical compression ratio is usually chosen below 12-14 and 10-12 for naturally aspirated and turbocharged engines, respectively. For the same reason, especially at high load, the Spark Advance (SA) has to be limited below a certain value (the Knock-Limited-Spark-Advance, $KLSA$), depending on the specific load-speed condition. Correspondingly, the combustion phasing expressed by the 50% Burned Mass Fraction, MFB_{50}, is delayed up to the knock-limited value, (the Knock-Limited-MFB_{50} - $KLMFB_{50}$).

The definition of those parameters must be very carefully selected in order to ensure a certain knock safety margin. At the same time, however, a relevant reduction of the thermal efficiency and of the power output must be paid. Knock phenomenon is for this reason widely recognized as one of the major barrier obstructing the further improvement of the engine thermal efficiency [1,2].

Different knock suppression strategies, such as mixture over-fuelling, fuels with higher octane number [2], cooled Exhaust Gas Recirculation (EGR) [3], water injection [4,5], cooling of the intake air, and turbulence enhancing [1], have been studied by experimental and theoretical points of view. Their impact on the improvement of the knock resistance may consistently vary, depending on the engine architecture, fuel composition, and operating conditions. Moreover, to get the maximum efficiency at high load, given the need to operate as close as possible to the knock borderline, a precise theoretical description and identification of the knock phenomenon is of great interest.

It is generally accepted that the most accurate representation of the complex Auto-Ignition (AI) processes is obtained with the solution of detailed chemical kinetic schemes, implying hundreds of species and thousands of reactions [6]. Only such kinetic schemes are able to correctly handle the properties of the reactive mixture, to consider the presence of intermediate species leading to the development of cool flames, or to reproduce the Negative Temperature Coefficient (NTC) regime, where mixture reactivity is mitigated by an increasing temperature. They are also able to supply information on the auto-ignition characteristics of pure or commercial fuels, requiring a

reliable surrogate definition in the latter case. The obvious drawback of this methodology in industrial applications is the excessive CPU time requirements.

To overcome this difficulty, simpler modelling approaches are also proposed in the literature. They are based on empirical formulations of auto-ignition delay, described by Arrhenius-type functions, and coupled to Livengood-Wu integral [7]. The auto-ignition delay can be measured in rapid compression machines and shock tubes or, alternatively, it can be computed by previously cited detailed chemical schemes at different pressures, temperatures and equivalence ratios. The introduction of the AI correlation within the Livengood-Wu integral then allows to take into account pressure and temperature variations during the auto-ignition process [2]. The main disadvantage of such formulation is the weakness in reproducing the NTC regime, and a limited possibility to utilize the correlation out from air/inert/fuel proportions considered for the correlation development. An additional drawback is the poor predictivity of the chemical effects induced by advanced knock suppression strategies, such as EGR or water injection.

While the above methodology is widely diffused in most of the commercially available 0D/1D models, an alternative procedure, based on the tabulation of kinetics, has been employed since some years in 3D CFD codes, where directly solving thousands of reactions and transporting the hundreds of related species is not affordable. The tabulation approach relies on the off-line solution of chemical reactions in a Constant-Pressure (CP) or Constant Volume (CV) reactor, and on the storage of the results in look-up tables, which are then inquired during the CFD computation [8,9].

Different strategies have been developed for the chemistry tabulation. In [10], the sole AI delay time, τ_{AI}, is stored. This information, once retrieved from the table, is employed in the Livengood-Wu integral [7]. In such a way, it is only possible to estimate the instant of the knock event, while the intermediate heat release, up to AI occurrence, is not available. Alternatively, τ_{AI} can be utilized [11] to estimate the autoignition reaction progress, which is tracked by a passive transported precursor scalar, based on the correlation by Lafossas [12]. More complex tabulation strategies involve the storage of both τ_{AI} and the time derivative, $\dot{c}$, of a synthetic auto-ignition progress variable, c. This technique, known as Tabulated Kinetic of Ignition (TKI) can be well integrated in the existing 3D-CFD combustion models, such as ECFM [8,13]. Other approaches entail the storage of both High-Temperature and Low-Temperature delay times, τ_{HT} and τ_{LT}, respectively [9], and of the reaction rates. Still more complex strategies, such as the the in situ adaptive tabulation and the dynamic adaptive chemistry, involve the tabulation/retrieval of most important species, too [14].

In the authors' knowledge, the application of such methods in a 0D/1D model is rather limited. Its implementation, indeed, seems very powerful, since it would allow to preserve the details of the original complex kinetics, with a minimal impact on the computing time. In addition, tabulation and 0D/1D modeling coupling opens the possibility of a cylinder-by-cylinder knock estimation, even during transient engine maneuvers.

Based on the above discussion, in this paper, a TKI approach for the tabulated chemistry is followed. This method represents a good compromise between accuracy and complexity, since it allows to reconstruct the time-evolution of unburned zone temperature. The above information could be also useful in further 0D model applications, such as the description of a Spark-Assisted Compression-Ignition (SACI) combustion regime [15,16]. In [17], in fact, a first example of TKI application for SACI modelling is

reported. The TKI consistency is here verified against the outcomes of a direct solution of the chemical kinetics, both in a homogeneous reactor and in engine applications.

The paper is schematized as follows: preliminary, tabulated chemistry is set up in a homogeneous reactor, in terms of reaction scheme and gasoline surrogate selections. Two tables are generated, referring to the auto-ignition event in a CV and CP reactor, for different initial conditions, including pressure, temperature, equivalence ratio, residual and water contents. Then, an engine application is considered to validate the developed tabulated chemistry. To this aim, a downsized turbocharged engine architecture is examined, where the knock control is a critical issue at high load. A complete 1D model is developed in GT-Power™ software, integrated with refined sub-models of in-cylinder turbulence, combustion and heat transfer. Concerning the knock sub-model, both the proposed tabulated chemistry approach and a detailed one, based on the online solution of the chemical kinetic, are implemented into the simulations. Two operating points at high load and low speed are considered, and a spark advance sweep is realized. Then, to highlight the capability of the developed tables to correctly handle the common anti-knock solutions, further parametric analyses are carried out at various cooled-EGR rates and Water-to-Fuel (W/F) ratios. Finally, full load simulations are realized to identify the *KLSA* trends for the on-line and tabulated chemistry knock models. Numerical values are compared with the reference *KLSA* values for the turbocharged engine and for an additional naturally-aspirated architecture.

Tabulated chemistry set-up. Mechanism selection and gasoline surrogate definition

Scientific literature is plenty of papers proposing different chemical schemes for the oxidation of hydrocarbon fuels [18-25]. Mehl et al. [18] identified a comprehensive scheme (1389 species, 5935 reactions), which is also proposed in reduced variants at 639 x 3479 and at 312 x 1488 species and reactions, while maintaining an accurate prediction of τ_{AI}. Andrae et al. presented a series of detailed (1120 x 4160) [19] and semi-detailed mechanisms (138 x 633 [20], 159 x 734 [21]), validated also in a homogeneous charge compression ignition engine. Cai and Pitsch [22] proposed an automatically optimized mechanism, which can also handle gasoline/ethanol blends. The scheme retains a compact size (339 x 1690) and was successfully validated against experimental measurements. In [23], a simpler skeletal model (56 x 168) was verified by the comparison with experimental data over extensive ranges of equivalence ratio, temperature, and pressure. A very efficient mechanism (32 x 55) for iso-octane and n-epthane mixture was also developed by Keck [24, 25].

It must be considered that, also in a tabulated approach, highly detailed mechanisms [18, 21] still pose CPU time issues, since the table construction requires the solution of a great number of predefined initial conditions and mixture compositions (order of magnitude 50'000 to 100'000 cases). On the other hand, the selected scheme must be able to include some basic species of interest for ICEs. Under this point of view, it is widely accepted that a proper surrogate for a commercial gasoline must be composed at least of iso-octane, n-epthane and toluene (TRF), while, in the case of oxygenated fuel, ethanol has to be included, too. Moreover, some recent studies [26] indicate that the NO oxidation mechanism is also important, especially if EGR is concerned. Based on the above discussion, the semi-detailed Andrae mechanism [21] is selected in this work, by adding to its original version the reaction sub-mechanisms for ethanol and NO species. The employed scheme counts 185 species and 937 reactions.

Concerning the fuel composition, a TRF blend is considered, with the addition of olefines (diisobutylene, DIB-1) [27], holding for a not-oxygenated European gasoline with RON=95.6, MON=87, and H/C=1.807, according to Table 1.

Table 1. Composition of the considered surrogate fuel.

Specie	vol - %	mol - %
Iso-Octane (i-C_8H_{18})	47.0	39.2
N-Epthane (C_7H_{16})	14.0	13.2
Toluene ($C_6CH_5CH_3$)	32.0	41.5
DIB-1 (JC8H16)	7.0	6.1

Since in the ICEs some burned residuals are always present at intake valve closure, their composition must be also defined. In the following, the residual composition is assumed as the burned gas equilibrium one at the thermodynamic state of the reactor (pressure, temperature and equivalence ratio). Residuals are hence mainly composed of N_2, H_2O and CO_2.

AI calculation in a homogeneous reactor and AI table build-up

Once initial pressure, temperature and composition have been assigned, the chemistry evolution in a fixed mass (1 kg) homogenous reactor can be quantified in terms of the progress variable, c, here defined as:

$$c = \frac{T - T_0}{T_{ad} - T_0} \qquad (1)$$

where T is the temperature at time t in the reactor, T_0 is its initial value, and T_{ad} is the adiabatic flame temperature. As known, the chemistry development depends on the reactor configuration, being it at constant pressure or constant volume (Figure 1).
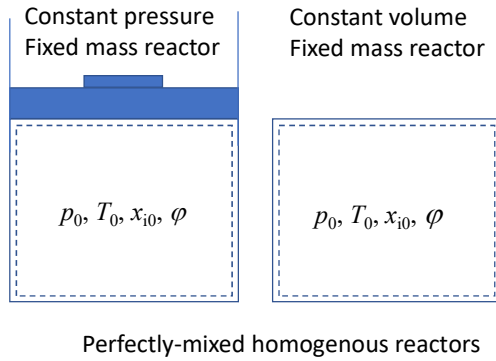

Figure 1. Schematization of a constant pressure (left) and a constant volume (right) reactor for assigned initial conditions.

Actually, both pressure and volume continuously vary in an engine and, for this reason, none of the above configurations exactly resembles the auto-ignition phenomenon in an ICE. However, many authors have utilized the information from either CP or CV reactors, although precise guidelines for the selection of one configuration are not yet clearly established in the literature. Usually, in Diesel engines, where the auto-ignition more likely takes place near the top dead center, within a small and almost constant volume, CV assumption is more frequent [28]. In SI engines, on the contrary, knock phenomena most likely occur at the end of the combustion

process, and the CP configuration is more frequently utilized [10,11]. Colin et al. [29, 30] put into evidence the errors included in a standard CP or CV case, and proposed a more complex variable volume tabulation, based on assigned positive and negative volume variations. Here, indeed, both CP and CV tables will be considered, and a comparison between them will be given to highlight the resulting differences under various operating conditions.

To describe the basics of the auto-ignition process in a homogenous reactor, in Figure 2a representative temperature profiles during time for both CP and CV configurations are depicted for two different initial conditions. Whichever is the initial thermodynamic state, as expected, the AI event in a CV reactor verifies earlier than the CP case. The figure also underlines that the adiabatic temperatures, reached at the AI process completion, differ between the CP and CV processes. The profiles in Figure 2b refer to the progress variable time evolution. In all cases, the variable reaches the unit, which indicates the complete auto-ignition occurrence. According to the initial condition and the rector configuration, the AI event verifies at a different time.

To implement a TKI approach, information about the progress variable derivative, $\dot{c}$, are stored at discrete c values. For each prefixed c_i, reached at time t_i, the derivate $\dot{c}_i$ is computed by a first-order forward equation:

$$\dot{c}_i = \frac{c_{i+1} - c_i}{t_{i+1} - t_i} \qquad (2)$$

Each row of the table is defined by an AI calculation at a prefixed initial condition. The first value of $\dot{c}$ is stored when c reaches a level of 10^{-7}, which is assumed as representative of the very first chemistry activation. The tabulation proceeds until the temperature reaches the adiabatic level, corresponding to c equal to the unit. Together with the progress variable derivative, also the time required for the chemistry activation is stored, τ_{init}.

An example of tabulated data at two different initial pressures and temperatures is shown in Figure 3, which depicts the $\dot{c}$ trends as a function of c. The figure puts into evidence the reaction speed-up during the process development, reaching the maximum level close to the AI onset. Moreover, although not visible in Figure 3, the occurrence of cool flames is captured, corresponding to local $\dot{c}$ peaks for a progress variable below 0.1.

The considered independent parameters for the table specification are the initial pressure and temperature, p_0 and T_0, the equivalence air/fuel ratio, φ, the residual mass fraction, x_r, and the W/F ratio. The latter parameter is of interest to also consider the chemical effects related to a water injection for knock mitigation [5, 31]. The extreme values of the independent parameters are selected to cover most of the conditions experienced in the in-cylinder unburned gas. The ranges and steps employed in this study are listed in Table 2. For each selection of initial conditions, $\dot{c}$ is tabulated for a fixed distribution of 99 c_i values. The overall AI table counts 221130 rows.

Table 2. Extreme levels and steps of the independent variables of the auto-ignition look-up table.

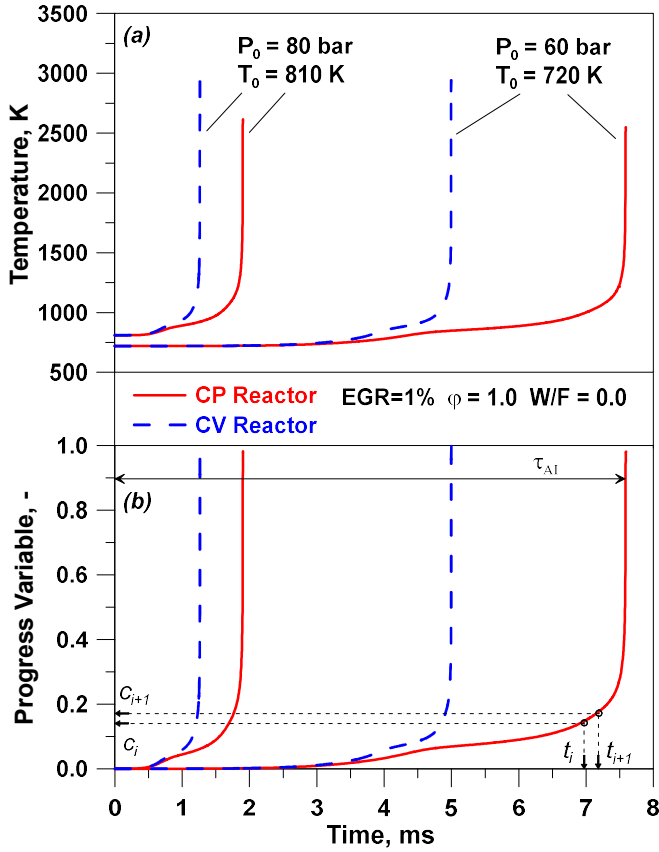|	Minimum	Maximum	Step
p_0, bar	10	150	10
T_0, K	600	1200	30
ϕ, -	0.4	1.6	0.1
x_r, -	0.0	0.4	0.05
W/F, -	0.0	0.5	0.1

Figure 2. Temperature (a) and progress variable (b) assessments between CP and CV reactors.
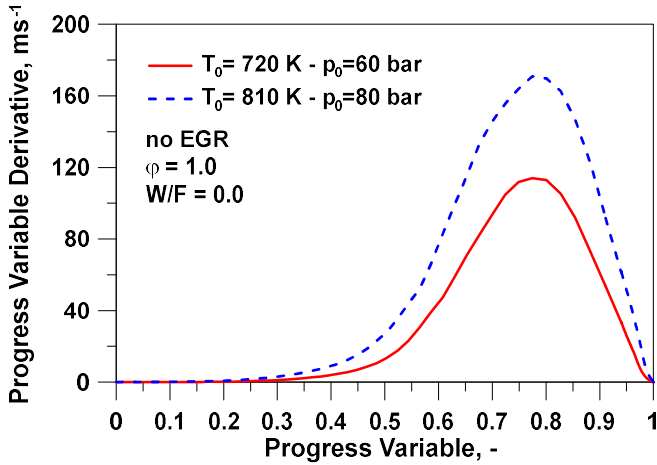

Figure 3. Progress variable assessment between CP and CV reactors.

TKI in a homogeneous reactor

To verify the consistency of the TKI approach, the assembled AI table is firstly utilized to perform an auto-ignition calculation in a homogenous reactor. This entails that, in each simulation, a single row of the table is inquired, the initial conditions being fixed. The procedure described below is also followed for variable pressure/temperature conditions, through the interpolation of AI table data.

As first step, the time required for the auto-ignition activation is computed:

$$\int_{t_0}^{t} \frac{dt}{\tau_{init}} \qquad (3)$$

When the integral expressed in Eq. (3) reaches the unit, the progress variable value is set as 10^{-7}, according to the assumption introduced in the previous section. From this time on, the progress variable is integrated following a Runge-Kutta fourth-order scheme, based on the progress variable derivatives extracted from the table interpolation. This datum is also used in the energy balance equation to compute the amount of heat released by the on-going AI process. The quantity $\dot{c}\Delta t$ is interpreted as the fraction of air/fuel gas which burns in the time step Δt. It is also utilized to update the composition of most important burned gas species, namely CO_2, H_2O, N_2, O_2, CO, H_2, H, O, OH, NO, N. Taking into account the AI heat release, the thermodynamic state evolves during the simulation, until the adiabatic temperature is reached, and the progress variable attains the unit. To check the reliability of the c integration, the evolution of the progress variable and of the thermodynamic state are compared to the corresponding trends, derived by an on-line chemistry computation.

A first assessment between kinetics (*kin*, continuous line) and TKI (*tab*, circles) is represented in Figure 4. The latter shows the time evolution of the progress variable at different pressures, temperatures, and EGR amounts in a CP reactor. Analogous results are depicted in Figure 5 for a CV configuration. The tabulated calculation results are in perfect agreement with the on-line outcomes. The auto-ignition time, namely the time when c reaches the unitary level, is precisely predicted by the simplified approach. The possibility of integrating the sole progress variable, instead of the hundreds or thousands of chemical reactions, allows to obtain very similar overall results, but with a drastically computational effort (a speed-up of about 1:8 is gained). Some discrepancies indeed emerge in the prediction of the instantaneous thermodynamic state. As an example, referring to the CP reactor, the comparisons between on-line and tabulated chemistry of the instantaneous temperature and density are plotted in Figure 6 and Figure 7, respectively. It can be observed that the profiles are superimposed at the beginning of the reaction progression and tend to slightly diverge before the auto-ignition onset. The tabulated approach slightly underestimates the temperature and overestimates the density. This is due to differences in the species concentration, turning in varied thermodynamic properties of the evolving fluid. Despite of the above-mentioned differences, the methodologies behave in a very similar way, and the AI occurrence verifies at the same time. Hence, tabulated method can be considered adequately accurate, assuming as a reference the on-line chemical calculation.

To further check the consistency of the tabulated approach, the isolated influence of EGR, equivalence ratio, and W/F ratio is shown in Figure 8, Figure 9 and Figure 10, respectively, with reference to the CV reactor. In all cases, the variations in the auto-ignition process follow the theoretical expectations, and the tabulated chemistry outcomes perfectly agree with the on-line chemical kinetic ones. It is interesting to note how the water presence in the unburned gases also exerts a certain chemical effect on the AI time, especially at lower pressure and temperature.
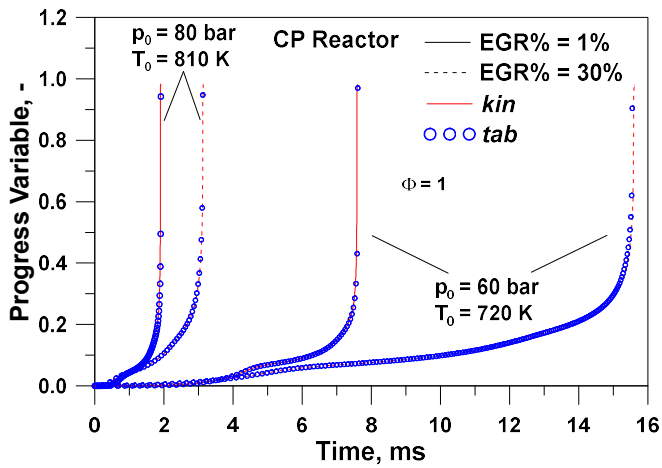
Figure 4. Progress variable assessment between detailed and tabulated chemistry at different EGR rates in a CP reactor.
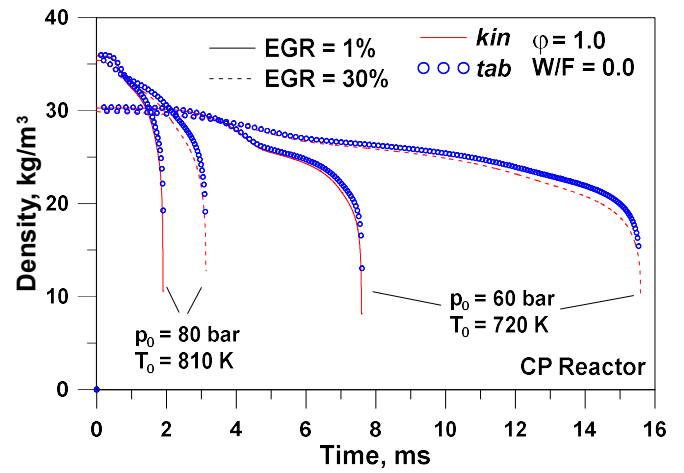

Figure 7. Density assessment between detailed and tabulated chemistry at different EGR rates in a CP reactor.
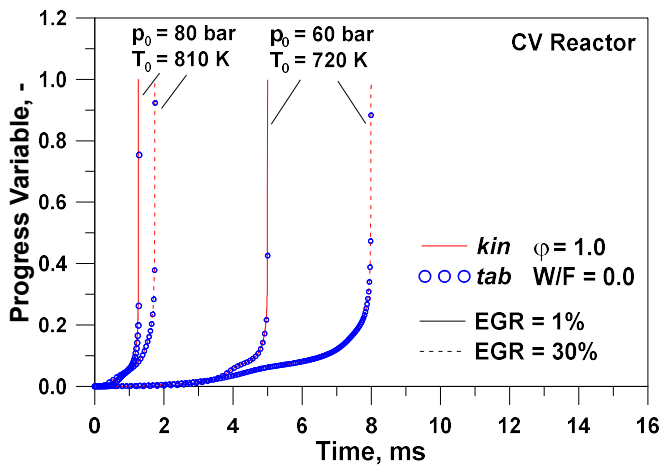

Figure 5. Progress variable assessment between detailed and tabulated chemistry at different EGR rates in a CV reactor.
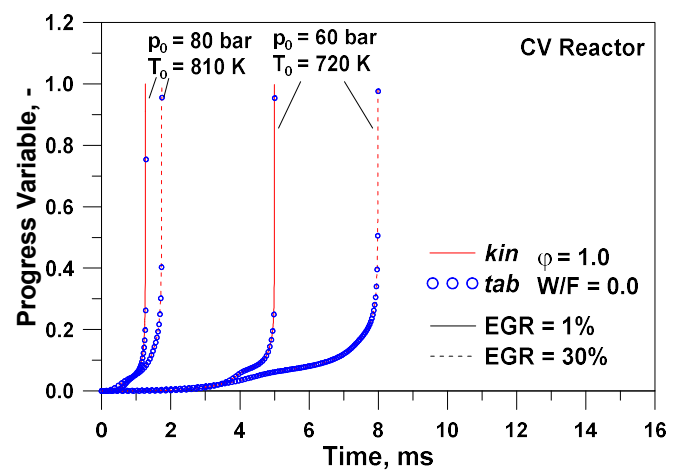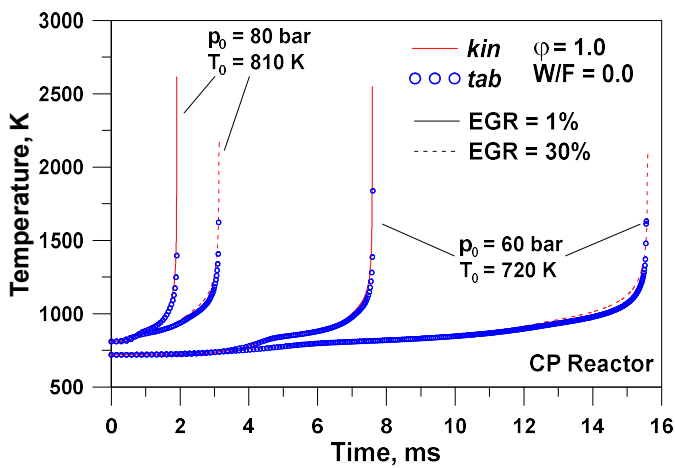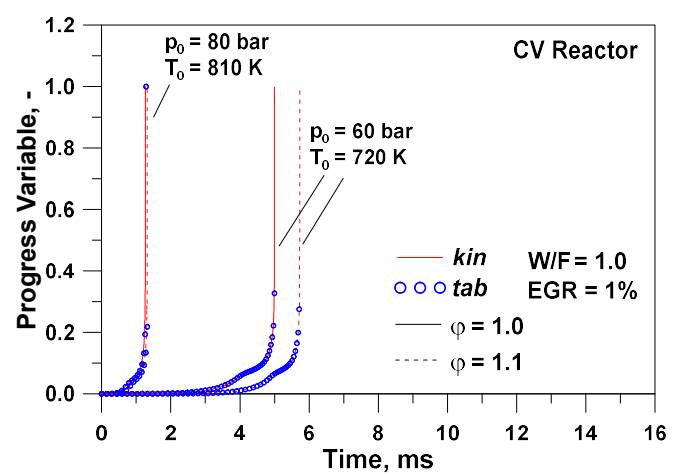

Figure 8. Progress variable assessment between detailed and tabulated chemistry at different EGR rates in a CV reactor.

Figure 6. Temperature assessment between detailed and tabulated chemistry at different EGR rates in a CP reactor.

Figure 9. Progress variable assessment between detailed and tabulated chemistry at different equivalence ratios in a CV reactor.
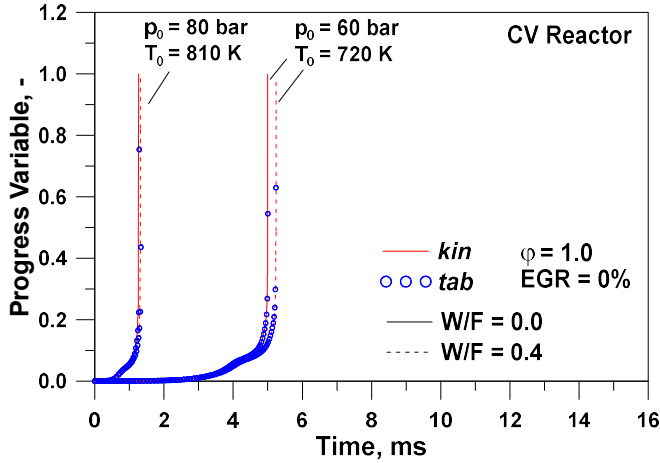
Figure 10. Progress variable assessment between detailed and tabulated chemistry at different water-to-fuel ratios in a CV reactor.

Engine architectures and experimental tests

The comparisons between TKI and on-line kinetics are extended to the analysis of ICEs, applied to knock prediction. Two engines are investigated, named "Engine A" and "Engine B": the first is a VVA Waste-Gated (WG) turbocharged PFI SI engine. Engine B, is a naturally aspirated PFI SI engine. Both engines have a pent-roof combustion chamber, with a centered spark-plug and include an EGR circuit. Engine A is also equipped with a water injector in the plenum pressure for knock mitigation.

An extended experimental campaign is performed on the engines, and full- and part-loads are investigated. The instrumentation of the test bench allows to measure both the overall performance data (fuel flow, Air-to-Fuel ratio – A/F, torque, and fuel consumption) and the in-cylinder pressure cycles. The latter are post-processed by an inverse analysis to derive the combustion data, such as the burn rate profiles and the characteristic combustion angles, namely MFB_{10}, MFB_{50} and MFB_{90}.

In the experimental tests at full load, the A/F ratio is properly enriched to limit the temperature at the turbine inlet for Engine A and at the TWC inlet for Engine B. The spark timing is selected to realize the maximum brake torque conditions, in case of knock-free operations, or it is properly delayed to control the knock intensity. For both the engines, this is the condition most frequently experienced at full load, causing delayed not-optimized combustion phasing. This is even more true for Engine A, because of the boosting needed to reach the performance target.

Engine model description

The tested engines are schematized in detail in the GT-Power environment. The numerical approach is based on the 1D description of the flow inside the intake and exhaust pipes and on the 0D modelling of the in-cylinder processes. The schematization includes the cylinders, the whole intake and exhaust systems, the throttle valve, and the EGR circuit (composed of a valve and of an EGR cooler). For Engine A, the waste-gated turbocharger is described by a conventional map-based approach, where the WG opening is adjusted to reproduce a measured datum (air flow rate, engine load or boost pressure). Different modalities are implemented to define the SA. It can be directly imposed (for instance, equal to the experimental

value), or automatically modified to match a prescribed MFB_{50} or a certain knock index level.

A refined model of the heat transfer inside the cylinder and for exhaust pipes is also employed, applying a wall temperature solver based on a finite element approach. Concerning the in-cylinder heat transfer, a Woschni-like correlation is used, while convective, radiative and conductive heat transfer modes are considered for the exhaust pipes. The combustion process is modeled through a two-zone "fractal approach" [32], where the burn rate is computed as:

$$\frac{dm_b}{dt} = \rho_u A_T S_L \qquad (4)$$

ρ_u being the unburned gas density, A_T the area of the turbulent flame front and S_L the laminar flame speed. The latter is computed by the correlation presented in [5]. Concerning the turbulent flame area, following the fractal geometry theory [33,34], it is derived by the laminar one, A_L, according to a wrinkling rate, which depends on the flame fractal dimension and on characteristic wrinkling scales. For the estimation of A_L, the flame front is described as a smooth spherically-shaped surface and its area is computed by an automatic procedure implemented in a CAD software. The latter processes the real 3D combustion chamber geometry to tabulate the laminar flame area as a function of the flame radius and of the in-cylinder volume. The estimation of the fractal dimension and of the wrinkling length scales is based on a turbulence sub-model, extensively reported in [35, 36].

The knock is computed with reference to a representative *faster-than-average* pressure cycle, rather than to the average cycle. This choice is widely confirmed by the experimental observations, suggesting that the knock phenomenon most likely verifies for the faster cycles of a sequence. The *faster-than-average* cycle is estimated starting from the average cycle and mimicking the experimental cyclic dispersion of the in-cylinder pressure peak. The knock event is conventionally assumed in the model as a sudden jump in the unburned temperature profile, as well as, a sudden increase in the pressure profile, due to the activation of "high temperature" reactions in the unburned gas zone.

From an experimental point of view, in case of knocking combustions, the measured in-cylinder pressure cycles show typical "high frequency" fluctuations, because of the wave reflections in the combustion chamber. The above discussed behavior cannot be described by a zero-dimensional approach, since the pressure propagation in the combustion chamber cannot be reproduced. Despite this model limitation, a jump in the numerical pressure profile can be detected, which can be related to the knock intensity. The knock index here employed represents the pressure increase, Δp_{knock}, computed assuming an instantaneous isochoric combustion of the end-gas still unburned at knock event:

$$\Delta p_{knock} = \frac{R}{c_v} \frac{x_{u,knock} \, m_f \, LHV}{V_{knock}} \qquad (5)$$

R and c_v being the average gas constant and the constant volume specific heat of the in-cylinder gases, m_f and LHV being the mass and the low heating value of the fuel, V_{knock} and $x_{u,knock}$ being the in-cylinder volume and end-gas unburned fraction at the knock event [37]. The considered formulation of the knock index closely resembles the experimental MAPO definition, as deeply discussed in [38].

Assessment of tabulated and chemical solver techniques on a SI engine

In this section, some parametric analyses are proposed to assess the tabulated and the on-line auto-ignition calculations for an engine application, rather than for a simpler homogeneous reactor case. In this case, in fact, the boundary conditions (pressure and temperature) continuously change because of the piston motion, combustion evolution, and heat transfer. For this reason, the employment of the CP or CV tables for the knock calculation is not straightforward to precisely reproduce the outcomes of the most accurate on-line chemistry methodology. Both the tables are here used to realize the knock prediction, and the results are compared with the detailed chemistry.

A first parametric analysis is carried out in the operating point at 2000 rpm and 18 bar BMEP. Keeping fixed the throttle valve position, the A/F ratio and the valve timing, a spark timing sweep is carried out, with a maximum SA of 25 CAD before the FTDC and a delayed limit of 10 CAD AFTDC. The highest SA is however constrained because of the attainment of the maximum allowed in-cylinder peak pressure. The prescribed BMEP level is realized in each case by adjusting the WG valve opening by an automatic PID controller. The throttle valve is assumed fully opened. The resulting numerical knock index, Δp_{knock}, is plotted against the SA in Figure 11. The latter compares the predicted knock intensities by the on-line and tabulated approaches. It can be observed that, for the considered operating point, a good agreement between the on-line chemistry and the CP table outcomes is reached. As expected, high knock intensities are predicted at SA increasing. To better describe the knock prediction methodology, in Figure 12-Figure 14 the burned and unburned temperature profiles, T_b and T_u, are depicted for representative spark timings, namely 10, -5 and -15 CAD AFTDC. In the first plot (Figure 12), all the methodologies forecast the same temperature profiles. Such a late spark timing, in fact, does not promote the auto-ignition reactions in the unburned zone, resulting in a null knock. Increasing the spark advance (SA = -5 CAD AFTDC), the unburned temperature profiles present substantial differences. It can be observed that T_u exhibits for all the methodologies a jump, highlighting the knock occurrence. The earlier the jump, the higher is the predicted knock intensity. The figure puts into evidence that the tabulated approach at constant pressure better agrees with the on-line chemistry, also providing a similar knock index (see Figure 11).
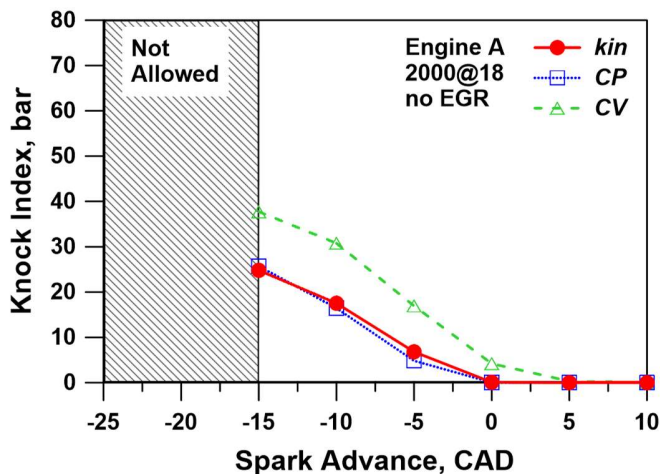

Figure 11. Knock index for different spark advances without external EGR. Assessment between on-line and tabulated chemistry.
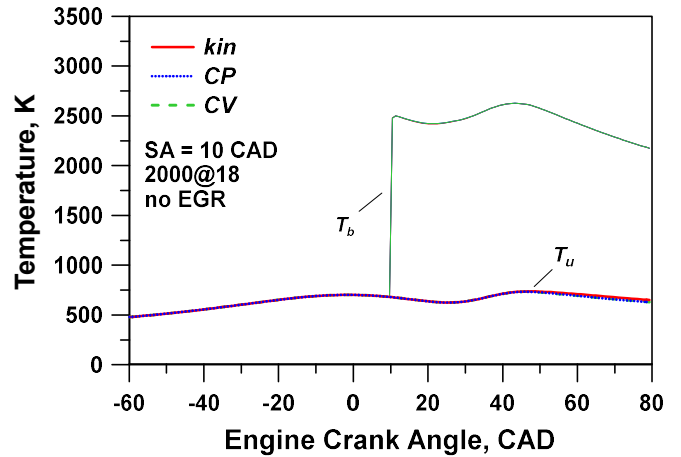

Figure 12. Assessment of burned and unburned temperatures profiles between on-line and tabulated chemistry for a SA= 10 CAD AFTDC without external EGR.
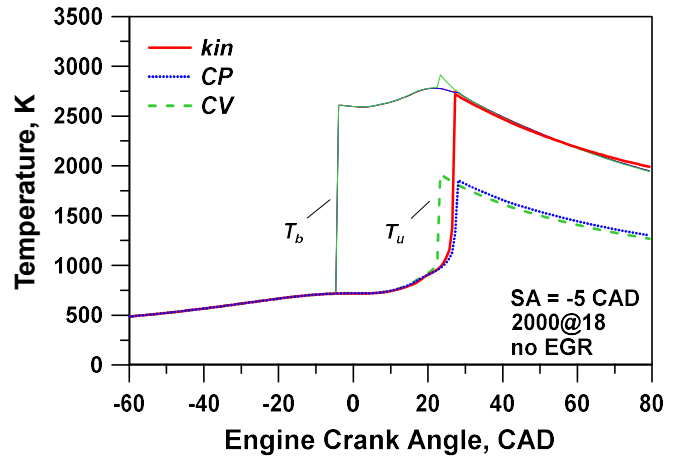

Figure 13. Assessment of burned and unburned temperatures profiles between on-line and tabulated chemistry for a SA= - 5 CAD AFTDC without external EGR.
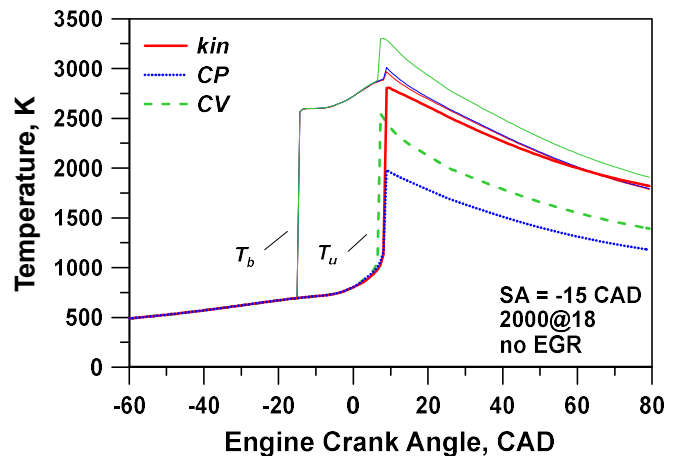

Figure 14. Assessment of burned and unburned temperatures profiles between on-line and tabulated chemistry for a SA= -15 CAD AFTDC without external EGR.

Advancing the spark timing up to -15 CAD AFTDC (Figure 14), the unburned temperature trends have the jump at very similar crank angles. This occurs very early during the engine cycle, just after the FTDC. Once again, the CP table better agrees with the on-line chemistry, compared to the CV outcomes. Based on the presented parametric study, the CP approach seems to represent the best solution to mimic the detailed chemistry in engine applications.

Further parametric analyses are carried out at increasing EGR rates (from 0 to 15%) and W/F ratios (from 0 to 0.6). In those simulations, the SA is no more assigned, but is automatically adjusted to identify the $KLSA$ and the $KLMFB_{50}$ realizing an assigned threshold level for the knock intensity (1.2 bar). The resulting $KLSA$, $KLMFB_{50}$, together with the boost pressures needed to meet the prescribed load, are plotted in Figure 15 and Figure 16, for EGR and WI strategies, respectively. They confirm that the CP tabulated chemistry gives the better agreement with the on-line calculations. Figure 15 puts into evidence that the EGR only marginally allows to advance the combustion phasing ($KLMFB_{50}$), denoting a reduced knock-suppression capability. On the other hand, the spark timing has to be advanced to compensate the inert-induced combustion lengthening. Conversely, as shown in Figure 16, the water addition allows to substantially advance the combustion phasing and spark event, thanks to its relevant knock mitigation capability [5, 31]. The combustion duration is only marginally affected by the water introduction. When the external EGR is applied, a certain boost compensation is necessary to maintain the same load level. The boost increase contributes to mask the EGR knock suppression potential. In the case of water injection, no boost compensation is required and, indeed, it has to be reduced to match the prescribed load.
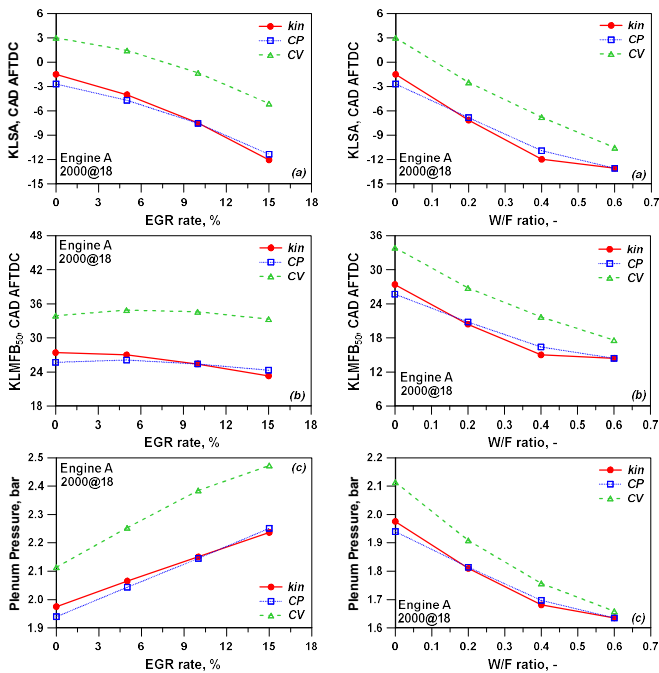

Figure 15. $KLSA$, $KLMFB_{50}$ and boost pressure at increasing EGR rates, resulting from on-line and tabulated chemistry

Figure 16. $KLSA$, $KLMFB_{50}$ and boost pressure at increasing W/F rates, resulting from on-line and tabulated chemistry.

The presented analyses allow to draw some main considerations:

- For the selected point, the CP tabulated approach better mimics the behavior the detailed chemistry.
- The tabulated methodology is equivalent to the on-line approach in the capability to sense the variations of the operating

parameters such as spark timing, in-cylinder pressure and temperature, inert and/or water content.

To verify if the above considerations are generally valid, the same parametric analyses are repeated in a different operating point, characterized by a higher load level, namely 20 bar BMEP, which represents the full load for the rotational speed of 2100 rpm. The corresponding knock index results are plotted in Figure 17.
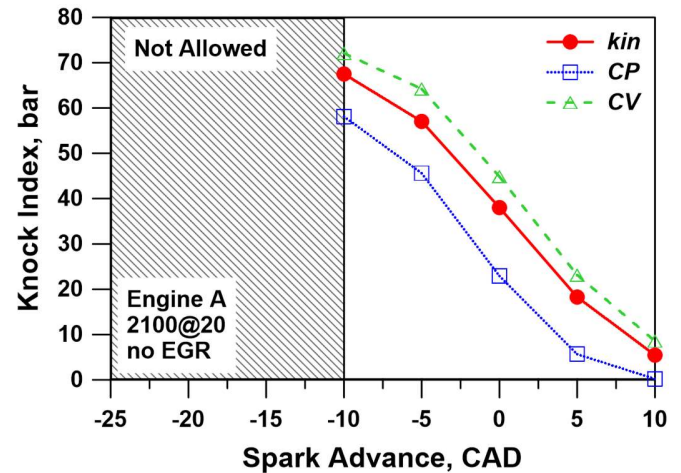

Figure 17. Knock index for different spark advances at higher load. Assessment between on-line and tabulated chemistry.
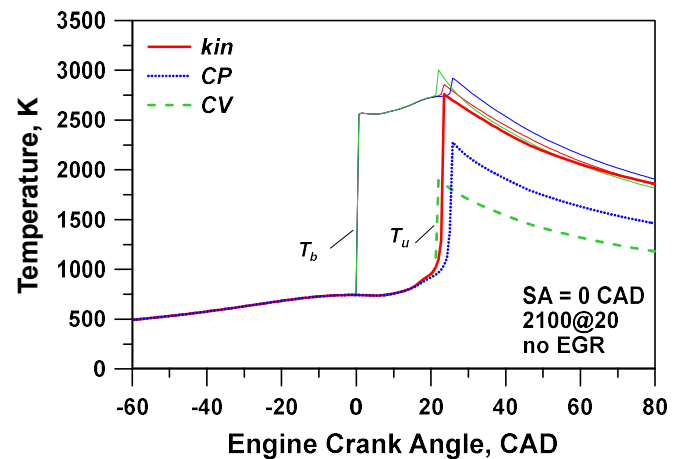

Figure 18. Assessment of burned and unburned temperatures profiles between on-line and tabulated chemistry for a SA= 0 CAD, at higher load

As a first observation, comparing it with Figure 11, it emerges that the predicted knock intensity is much higher for a fixed spark timing. The more interesting difference with the case at lower load relays in the fact that the knock index predicted by the CP table is no more in good agreement with the on-line chemistry output. For all the SA, the on-line chemistry-derived Δp_{knock} assumes a level closer to the CV tabulated one. As a matter of fact, at the higher load, cool flames more frequently occur, as it can be clearly seen in Figure 18. They probably increase mixture reactivity and determine an earlier auto-ignition.

The same discrepancy is also found in other operating points at full load. The above observations seem to confirm the analyses carried out in [9], where a specific delay time for low temperature reaction and a related small heat release is tabulated, too. They are utilized to enter the AI table at a higher temperature when the cool flames take

place. The same strategy will be also attempted in the present research activity in the next developments of the methodology.

At the moment, however, it is always found that the on-line chemistry results lie in between CP and CV outcomes, representing lower and upper knock bounds. As a general rule, the presented analyses indicate that the proper selection of the tabulated approach for a SI engine is the CP configuration. On the other hand, some knock underestimation can be expected at very high load, probably due to low-temperature heat release. The highlighted uncertainties can be easily overcome by a proper selection of threshold level for the knock intensity, as discussed in the next section.

Full load analyses and KLSA identification

Here the knock model is applied to numerically identify the *KLSA* for two different SI engines at full load. Preliminary, full load torque is predicted for Engine A and B imposing the measured setting of the control variables. In particular, the experimental A/F ratios and valve strategies are specified in the model. The throttle valve is assumed fully opened. The WG valve of engine A is controlled by a PID to match the measured boost level. The spark timing is automatically adjusted to realize the experimental combustion phasing (*MFB50*). To prove the model reliability in predicting the global engine performance, the numerical/experimental comparisons of brake torque and volumetric efficiency are shown in Figure 19 and Figure 20, respectively. The agreement is satisfactory for both engines, with minor discrepancies on Engine B, mainly due to an inaccurate prediction of the volumetric efficiency in the medium-speed range.
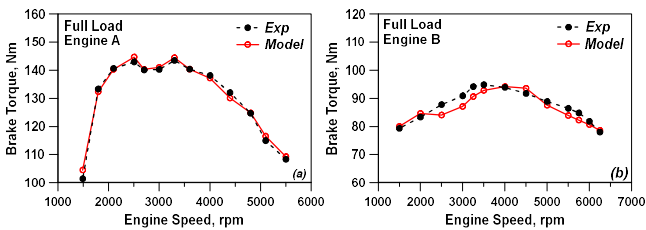

Figure 19. Numerical/experimental assessment of brake torque at full load for engine A (a) and engine B (b).
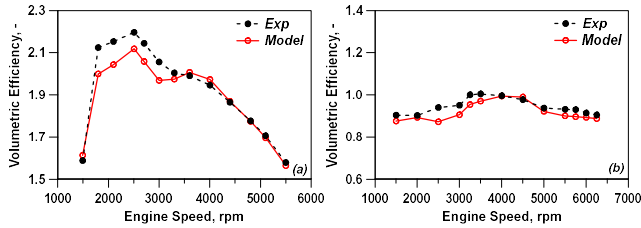

Figure 20. Numerical/experimental assessment of volumetric efficiency at full load for engine A (a) and engine B (b).
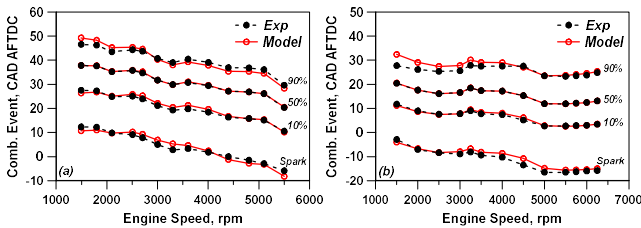

Figure 21. Numerical/experimental assessment of characteristic combustion angles at full load for engine A (a) and engine B (b).

An insight in the combustion process description is given by the comparisons of the characteristic combustion angles, namely spark, *MFB10*, *MFB50*, *MFB90*, depicted in Figure 21. The combustion and turbulence sub-models prove an adequate reliability in describing the combustion evolution over the whole full load curve, without requiring any case-dependent tuning. The above results indicate that the engine model is correctly schematized, and the adopted sub-models behave in a reliable way.

Starting from this point, and assuming that both engines are working at full-load at the knock borderline, the knock model is activated to estimate the *KLSA*. To this aim, a proper knock threshold level has to be selected. Since this value is unknown at this stage, a parametric analysis is carried out for Engine A. The simulations are repeated for on-line and CP tabulated chemistry, with *Δpknock* limits of 1, 3 and 5 bar. The resulting *KLSA* are plotted in Figure 22. They are compared to reference values, derived in the *MFB50*-imposed simulations shown in Figure 21 (*ref* profiles in the next figures). In this way, the sole knock model accuracy is checked, without introducing additional uncertainties related to the combustion simulation.

As expected, whichever is the chemistry computational method, a higher *Δpknock* threshold determines more delayed spark timings. The results in Figure 22a underline that the best agreement with the reference SA is obtained with a threshold level of 1 bar in case of CP tabulated chemistry, while the optimal *Δpknock* in case of on-line chemistry is 5 bar. Similar analyses for engine B, not reported here for sake of brevity, show that the optimal threshold level is 1 bar for the tabulated CP chemistry and 4 bar for the on-line computation.
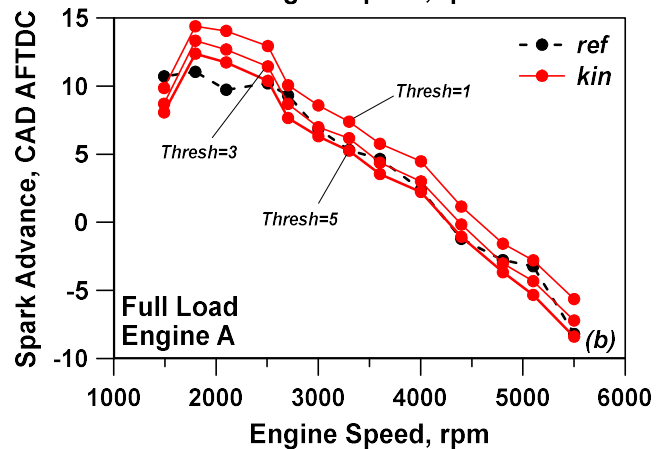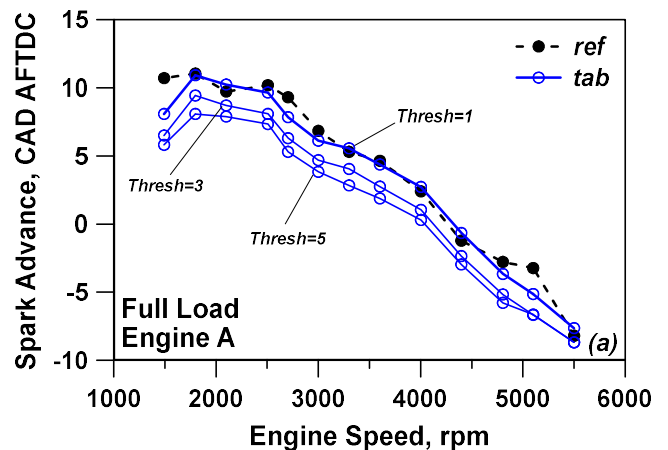

Figure 22. Parametric analysis on the knock threshold for tabulated (a) and on-line (b) approaches. *KLSA* calculation at full load for Engine A.

The above threshold adjustment, which might be considered as a knock model tuning procedure, is a consequence of high load discrepancies highlighted between TKI and on-line methodologies. The identified optimal Δp_{knock} values are within a range of few bars, which are similar to MAPO levels usually specified in the engine calibration at the test bench.

In Figure 23, reference, tabulated and on-line *KLSA* calculations are finally compared for both engines, utilizing for each case the optimal related threshold value. Whichever is the knock modeling, a good agreement with reference *KLSA* values is obtained. Concerning Engine A, the maximum absolute *KLSA* difference is about 2.6 CAD for both the on-line model and the tabulated one. For Engine B, similar maximum absolute errors are achieved (2.3 CAD and 1.4 CAD for on-line and tabulated models, respectively). The maximum *KLSA* difference between on-line and tabulated approaches is indeed 1.5 CAD for Engine A and 0.8 CAD for engine B. It is hence demonstrated that the two knock modeling approaches provide similar outcomes, confirming the possibility of employing the tabulated methodology, rather than the much more time-consuming detailed chemistry, maintaining the same reliability. However, in both cases, a preliminary threshold selection phase is mandatory to get the optimal results.
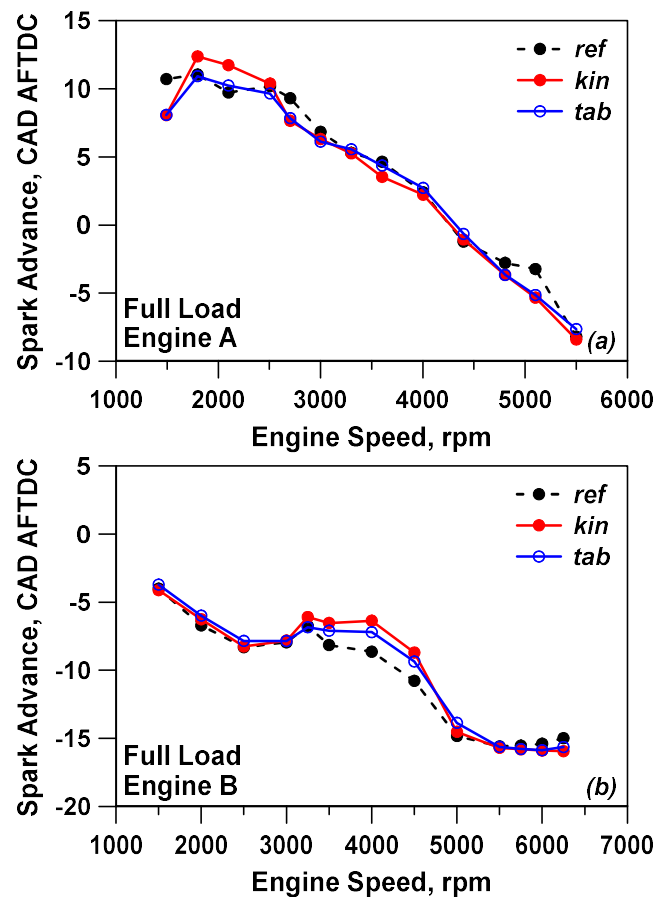

Figure 23. Assessment among reference, tabulated and on-line *KLSA* calculations at full load for Engine A (a) and for Engine B (b).

As a final remark, the methodology based on the tabulated chemistry showed the capability to reliably predict the onset of knocking combustions and hence the spark advance at knock borderline. Compared to the on-line chemistry approach, no evident loss of accuracy is highlighted. The computational time speed-up is indeed

relevant, and it is confirmed to reach a ratio of about 1:8, as in the homogenous reactor analyses. Of course, the overall computing time depends on engine architecture and simulation strategy. Actually, for a *KLSA* identification in a turbocharged engine, such as Engine A, hundreds of computing cycles are required to attain the turbocharger torque equilibrium and to stabilize the spark-advance PID at the selected threshold. That means that huge advantages on the overall computational time are achieved, especially for Engine A.

Conclusions

The paper describes the development and the validation of a knock model, based on tabulated chemistry, integrated in a phenomenological combustion model for SI engines. The methodology is also compared with a more sophisticated approach, based on the on-line resolution of chemistry by a semi-detailed chemical kinetic solver. The development of this tabulated methodology relays in the need to maintain an accurate knock prediction, expected to be similar to the detailed chemistry one, but with a very reduced computational effort.

In a first stage, the tabulated methodology has been verified in a simplified test case, namely in a homogeneous reactor, with fixed initial conditions (pressure and temperature) and composition (air/fuel ratio, residual and water contents). In these preliminary analyses, a very good agreement with the detailed chemistry resolution has been observed. The simulations have concerned both constant pressure and constant volume reactors.

In a second stage, the tabulated approach, used for the knock detection, has been verified in various "on-engine" applications, and compared to the on-line chemistry. To this aim, a waste-gated turbocharged engine, equipped with an external EGR circuit, has been selected and some parametric analyses have been performed at constant loads. The numerical investigations have regarded sweep of spark advance (w/ and w/o EGR), gas recirculation rate and water injection amount. The simulations have pointed out the capability of the methodology in sensing the knock intensity variations at changing boundary conditions, following trends in agreement with the on-line chemistry and physical expectations.

The presented results have shown that the CP tabulation can be preferred with respect to CV configuration. A knock intensity underestimation can however occur at very high load, due to the impact of the low-temperature reactions. Additional activities are ongoing to include cool-flames heat release, to modify the thermodynamic properties of the unburned zone, utilized to access the AI table. Nevertheless, at present stage of the research, the calculations at different knock thresholds have shown that an accurate *KLSA* identification can be still realized, through the selection of an appropriate knock limit.

The proposed methodology has demonstrated to behave in a very similar way as the detailed chemistry, but requiring reduced computational effort (speed-up ratio 1:8 in most cases). It can hence represent a very effective and efficient methodology to support and drive the engine development and calibration, also from an industrial point of view.

References

1. Zhen, X., Wang, Y., Xu, S., Zhu, Y., Tao, C., Xu, T., Song, M., "The engine knock analysis – An overview," *Applied Energy* 92: 628-636, 2012, doi: 10.1016/j.apenergy.2011.11.079.
2. Kalghaltgi, G., "Knock onset, knock intensity, superknock and preignition in spark ignition engines," *International J. of Engines Research*, 19(1): 7-20, 2018, doi: 10.1177/1468087417736430.
3. Wei, H., Zhu, T., Shu, G., Tan, L., Wang, Y., "Gasoline engine exhaust recirculation – A review," *Applied Energy* 99:534-544, 2012, doi: 10.1016/j.apenergy.2012.05.011.
4. Hoppe, F., Thewes, M., Baumgarten, H., Dohmen, J., "Water injection for gasoline engines: Potentials, challenges, and solutions," *International J. of Engine Research* 17(1):86-96, 2016, doi: 10.1177/1468087415599867.
5. Bozza, F., De Bellis, V., Giannattasio, P., Teodosio, L., Marchitto, L., "Extension and Validation of a 1D Model Applied to the Analysis of a Water Injected Turbocharged Spark Ignited Engine at High Loads and over a WLTP Driving Cycle," *SAE Int. J. Engines* 10(4):2141-53, 2017, doi : 10.4271/2017-24-0014.
6. Lu, T., Law C., "Toward accommodating realistic fuel chemistry in large scale computations," *Progress in Energy and Combustion Science* 35(2):195-215, 2009, doi: 10.1016/j.pecs.2008.10.002.
7. Livengood, J., C., Wu, P., C., "Correlation of Autoignition Phenomena in Internal Combustion Engines and Rapid Compression Machines," *Symposium (International) on Combustion* 5(1):347-356, 1955, doi: 10.1016/S0082-0784(55)80047-1.
8. Knop, V., Michel, J., Colin, O., "On the use of a tabulation approach to model auto-ignition during flame propagation in SI engines," *Applied Energy* 88: 4968-79, 2011, doi: 10.1016/j.apenergy.2011.06.047.
9. Colin, O., Pires da Cruz, A., Jay, S., "Detailed chemistry-based auto-ignition model including low temperature phenomena applied to 3D engine calculations," *Proceeding of the Combustion Institute* 30: 2649-56, 2005, doi: 10.1016/j.proci.2004.08.058.
10. Breda, S., D'Adamo, A., Fontanesi, S., Giovannoni, N. et al., "CFD Analysis of Combustion and Knock in an Optically Accessible GDI Engine," *SAE Int. J. Engines* 9(1):2016, doi:10.4271/2016-01-0601.
11. D'Adamo, A., Breda, S., Fontanesi, S., Cantore, G., "A RANS-Based CFD Model to predict the statistical occurrence of Knock in Spark-Ignition engines," *SAE Int. J. Engines* 9(1):2016, doi:10.4271/2016-01-0581.
12. Lafossas, F., Castagne, M. , Dumas, J., Henriot, S., "Development and Validation of a Knock Model in Spark Ignition Engines using a CFD code," SAE Technical Paper 2002-01-2701, 2002, doi: 10.4271/2002-01-2701.
13. Lecocq, G., Richard, S., Michel, J-B., Vervisch, L, "A new LES model coupling flame surface density and tabulated kinetics approaches to investigate knock and pre-ignition in piston engines," *Proceeding of the Combustion Institute* 33: 3105-34, 2011, doi: 10.1016/j.proci.2010.07.022.
14. Ren, Z., Liu, Y., Lu, T., Lu, L., Oluwole, O., Goldin, G., "The use of dynamic adaptive chemistry and tabulation in reactive flow simulations," *Combustion and Flame*, 161:127-137, 2014, doi: 10.1016/j.combustflame.2013.08.018.
15. Martz, J., Kwak, H., Im, H., Lavoie, G., Assanis, D., "Combustion regime of a reacting front propagating into an auto-igniting mixture," *Proceedings of the Combustion Institute*, 33(2):3001-3006, 2011, doi: 10.1016/j.proci.2010.07.040.
16. Martz, J. , Lavoie, G. , Im, H. , Middleton, R. , Babajimopoulos, A., Assanis, D., "The propagation of a laminar reaction front during end-gas auto-ignition," *Combustion and Flame*, 159(6), 2077-2086, 2012, doi: 10.1016/j.combustflame.2012.01.011.
17. Bozza, F., De Bellis, V., Tufano, D., Malfi, E., Müller, C., Habermann, K., "A quasi-dimensional model of pre-chamber Spark-Ignition Engines," SAE Technical Paper 19PFL-0866, 2019.
18. Mehl, M., Pitz, W., Westbrook C., Curran, H., "Kinetic modeling of gasoline surrogate components and mixtures under engine conditions," *Proceeding of the Combustion Institute* 33: 193-200, 2011, doi: 10.1016/j.proci.2010.05.027.
19. Andrae, J., "Development of a detailed kinetic model for gasoline surrogate fuels," *Fuel* 87: 2013-22, 2008, doi: 10.1016/j.fuel.2007.09.010.
20. Andrae, J., " Kinetic Modeling of the Influence of NO on the Combustion Phasing of Gasoline Surrogate Fuels in an HCCI Engine," *Energy & Fuels* 27: 7098-7107, 2013, doi: 10.1021/ef401666c.
21. Andrae J., Kovàcs, T., "Evaluation of Adding an Olefin to Mixtures of Primary Reference Fuels and Toluene To Model the Oxidation of a Fully Blended Gasoline," *Energy & Fuels* 30: 7721-7730, 2016, doi: 10.1021/acs.energyfuels.6b01193.
22. Cai, L., Pitsch, H., "Optimized chemical mechanism for combustion of gasoline surrogate fuels," *Combustion and Flame* 162: 1623-37, 2015, doi: 10.1016/j.combustflame.2014.11.018.
23. Liu, Y-D., Jia, M., Xie, M., Pang B., "Development of a New Skeletal Chemical Kinetic Model of Toluene Reference Fuel with Application to Gasoline Surrogate Fuels for Computational Fluid Dynamics Engine Simulation," *Energy & Fuels* 27: 4899-4909, 2013, doi: 10.1021/ef4009955.
24. Hu, H., Keck, J., "Autoignition of Adiabatically Compressed Combustible Gas Mixtures," SAE Technical Paper 872110, 1987, doi:10.4271/872110.
25. Keck, J., Hu, H., "Explosions of Adiabatically Compressed Gases in a Constant Volume Bomb," Int. Symposium on Combustion, *The Combustion Institute* 21(1): 521-529, 1988, doi:10.1016/S0082- 0784(88)80281-9.
26. Pasternak, M., Netzer, C., Mauss, F., Fisher, M., Sens, M., Riess, M., "Simulation of the Effects of Spark Timing and External EGR on Gasoline Combustion Under Knock-Limited Operation at High Speed and Load," International Conference on Knocking in Gasoline Engines, 2018, doi:10.1007/978-3-319-69760-4_8.
27. Andrae, J., J A Reaction Engineering, Taby, Sweden, June 2018, personal communication.
28. Pera, C., Colin, O., Jay, S., "Development of a FPI Detailed Chemistry Tabulation Methodology for Internal Combustion Engines," *Oil&Gas Science and Technology* 64(3): 243-258, 2009, doi: 10.2516/ogst/2009002.
29. Jay, S., Colin, O., "A variable volume approach of tabulated detailed chemistry and its applications to multidimensional engine simulations," *Proceeding of the Combustion Institute* 33: 3065-72, 2011, doi: 10.1016/j.proci.2010.08.003.
30. Tudorache, D., "Chemical kinetics tabulation for pollutants prediction in internal combustion engines," Doctoral Thesis in Energétique, Ecole Centrale Paris, 2013.
31. De Bellis, V., Bozza, F., Teodosio, L., Valentino, G., "Experimental and Numerical Study of the Water Injection to Improve the Fuel Economy of a Small Size Turbocharged SI Engine," *SAE Int. J. Engines* 10(2):550-561, 2017, doi: 10.4271/2017-01-0540.
32. De Bellis, V., Bozza, F., Tufano, D., "A Comparison Between Two Phenomenological Combustion Models Applied to Different SI Engines," SAE Technical Paper 2017-01-2184, 2017, doi: 10.4271/2017-01-2184.

33. North, G., Santavicca, D., "The fractal nature of premixed turbulent flames", *Combustion Science and Technology* 72(4-6): 215-232, 1990, doi: 10.1080/00102209008951648.

34. Gatowsky, J., Heywood, J., "Flame Photographs in a Spark-Ignition Engine", *Combustion and Flame* 56:71-81, 1984, doi: 10.1016/0010-2180(84)90006-3.

35. De Bellis, V., Bozza, F., Fontanesi, S., Severi, E. et al., "Development of a Phenomenological Turbulence Model through a Hierarchical 1D/3D Approach Applied to a VVA Turbocharged Engine," *SAE Int. J. Engines* 9(1):506-519, 2016, doi:10.4271/2016-01-0545.

36. Bozza, F., Teodosio, L., De Bellis, V., Fontanesi, S. et al., "Refinement of a 0D Turbulence Model to Predict Tumble and Turbulent Intensity in SI Engines. Part II: Model Concept, Validation and Discussion," SAE Technical Paper 2018-01-0856, 2018, doi: 10.4271/2018-01-0856.

37. Bozza, F., De Bellis, V., Minarelli, F., Cacciatore, D., "Knock and Cycle by Cycle Analysis of a High Performance V12 Spark Ignition Engine. Part 2: 1D Combustion and Knock Modeling," *SAE Int. J. Engines* 8(5):2015, doi:10.4271/2015-24-2393.

38. De Bellis, V., Teodosio, L., Siano, D., Minarelli, F. et al., "Knock and Cycle by Cycle Analysis of a High Performance V12 Spark Ignition Engine. Part 1: Experimental Data and Correlations Assessment," *SAE Int. J. Engines* 8(5):2015, doi:10.4271/2015-24-2392.

Contact information

Acronyms

0D-1D-3D	Zero-One-Three-dimensional
A/F	Air-to-fuel ratio
AI	Auto-ignition
AFTDC	After firing top dead center
BMEP	Brake mean effective pressure
CAD	Crank angle degree/ Computer aided design
CFD	Computational fluid dynamics
CP	Constant pressure
CPU	Central processing unit
CV	Constant volume
DAC	Dynamic adaptive chemistry
ECFM	Extended Coherent Flame Model
EGR	Exhaust gas recirculation
FTDC	Firing top dead centre
ICE	Internal combustion engine
KLMFB$_{50}$	Knock limited MFB$_{50}$
KLSA	Knock limited spark advance
LHV	Low heating value of the fuel
MAPO	Maximum amplitude of pressure oscillation
MFB	Mass fraction burned
MON	Motor octane number
NTC	Negative temperature coefficient
PFI	Port fuel injection
PID	Proportional integral derivative controller
RON	Research octane number
SA	Spark advance
SACI	Spark Assisted Compression Ignition
SI	Spark ignition
TRF	Toluene reference fuel
TKI	Tabulated kinetic of ignition
TWC	Three way catalytic converter
VVA	Variable valve actuation
W/F	Water-to-fuel ratio
WG	Waste-gate valve

Symbols

A_L	Laminar flame area
A_T	Turbulent flame area
c	Progress variable of reactions evolution
$\dot{c}$	Progress variable derivative
c_v	Constant volume specific heat of the in-cylinder gases
Δp	Pressure increase
Δt	Time step
m_b	Burned mass
m_f	Fuel mass
p	Pressure
R	Average gas constant
S_L	Laminar flame speed
t	Time
T	Temperature
V_{knock}	In-cylinder volume at knock event
x_r	Residual gas fraction
$x_{u,knock}$	End-gas unburned gas fraction at knock event

Greeks

φ	Equivalence ratio
ρ	Unburned gas density
τ	Time delay

Subscripts

0	Related to initial condition
adiab	Related to the adiabatic condition
b	Related to burned gas
init	Related to the auto-ignition chemistry initiation
knock	Related to knock event
u	Related to unburned gas